Ceramics

Strength assessment of Al_2O_3 and $MgAl_2O_4$ using micro- and macro-scale biaxial tests

Jürgen Peter Gross[1],* (iD), Jürgen Malzbender[1], and Ruth Schwaiger[1,2]

[1] *Institute of Energy and Climate Research: Microstructure and Properties of Materials (IEK-2), Forschungszentrum Jülich GmbH, 52425 Jülich, Germany*

[2] *Chair of Energy Engineering Materials, RWTH Aachen University, 52056 Aachen, Germany*

ABSTRACT

The application of ceramics in advanced functional applications often requires thicknesses below a few hundred micrometers, rendering an assessment of the materials' strength particularly challenging. In this work, different testing methods are combined to elucidate the effect of the volume and the surface area of the specimens under tensile loading on the fracture strength of Alumina of different purities and Spinel. A ball-on-3-ball test has been implemented into a micro-indentation system permitting as novelty a high control and acquisition of loads and displacements to study the biaxial fracture stress of thin specimens. In addition, ring-on-ring tests are carried out for thicker specimens. Weibull statistics is applied to analyze the fracture stresses. Considering all individual data sets obtained using the two testing methods, the effective volume approach appears most suitable for the materials tested. This conclusion is confirmed by fractographic analysis, where pores could be identified as the main failure initiating defect. The combination of a micro-indentation system and a ball-on-3-ball test as micro-and macro-scale biaxial tests represents an easy, fast and reliable methodology to investigate small scale ceramic materials.

Introduction

Fracture strengths and failure probabilities are highly important characteristics to evaluate the reliability of functional ceramic materials [1, 2]. Hence, an accurate determination of the materials' fracture stresses and their statistical analysis is crucial. New challenges arise due to the application-driven ongoing trend toward thinner functional ceramic components. Well-established and widely used 3-point and 4-point bending tests as well as ring-on-ring (ROR) bending tests typically require rather thick specimens [3, 4], though. Furthermore, the 3-and 4-point bending tests exhibit drawbacks associated with the influence of edge defects, while the ring-on-ring testing geometry requires rather well prepared, flat and uniform discs [5, 6].

The ball-on-3-ball test (B3B) has been utilized in some studies, since it permits characterization of fracture stresses of thin specimens. Furthermore, the method is more tolerant regarding the uniformity of specimens [7]. The B3B test induces a well-defined stress field, where the highest stress exists in the center of the specimen. Hence, processing-induced damages at the specimen edges have no influence on the results [8]. However, an accurate measurement of the fracture load and a precise positioning of the test specimens are important to facilitate reliable results [7]. In fact, modern micro-indentation systems fulfill the necessary requirements regarding load control and positioning. Therefore, in the current work, as a novelty a B3B test has been implemented in a micro-indentation system.

Usually, fracture stresses are analyzed using Weibull statistics. This statistical approach yields the characteristic strength and the Weibull modulus and, thus, permits a derivation of failure probabilities for particular stress levels [2, 9, 10]. Weibull theory assumes that the probability of defects being present depends on the effective volume (for volume defects) or effective area (surface defects) [10, 11], which leads to differences in the reported results depending on the chosen reference. Predictions for components in different, especially application-relevant, dimensions therefore requires characterization of the characteristic strength, the Weibull modulus and the effective volume or surface area [12]. Consequently, verification and prediction becomes more accurate if characteristic strengths for different effective volumes and areas are available. However, such studies are limited [3], in particular for thin specimens with thicknesses of a few hundred micrometers and less. A recently published study revealed that B3B results are comparable to ROR values, however, the material thicknesses were > 1 mm [13]. Moreover, studies employing a small scale B3B tests and a subsequent fractographic investigation for specimens in the 100 μm range along with a comparison to another biaxial testing method for specimens in the mm range, which considers thus a significantly different effective volume and surface area, have not yet been reported.

In this work, fracture stresses of different ceramic materials, i.e., 92% and 99% pure Al_2O_3 and $MgAl_2O_4$ (Spinel), with different specimen thicknesses, are characterized by B3B and ROR tests. The individual data sets are analyzed using Weibull statistics. The analysis is extended toward considering effective volumes and surface areas with the goal to confirm the appropriateness of the test set-ups and methodologies and to present a foundation for the prediction of failure probabilities of application-relevant components.

Experimental

Two different commercially available Alumina materials (ALOTEC®99 and ALOTEC®92, CeramTec-ETec GmbH, Lohmar, Germany) as blocks with Al_2O_3 contents of 99.2 and 92%, respectively, were procured, in the following abbreviated as ALUMINA1 (ALOTEC®92) and ALUMINA2 (ALOTEC®99). Material properties are listed in [14].

Plates of average thicknesses of 120 and 250 μm were prepared using an Orbit 25 CNC grinding machine (BLOHM) with a diamond grinding disc of ~ 88 μm (D91) grain size and a C75 concentration. Afterward, the disc-shaped samples were extracted from the plates using a Typ22 STAE (Aciera) diamond hollow drill with an inside diameter of 3 mm, resulting in a total of 160 samples of different thicknesses with diameters of ~ 3 mm. Additional 45 specimens from ALUMINA1 as well as of ALUMINA2 blocks were prepared with an average thicknesses of 800 μm and a diameter of 12 mm for ROR testing. More details on the different test series are presented in Table 1.

In addition, commercially available polycrystalline Spinel, $MgAl_2O_4$ (Perlucor®, CeramTec-ETec GmbH, Lohmar, Germany) samples were used for the B3B experiments. The samples were delivered by the manufacturer in a disc shape with a diameter of 3 mm and a thickness of 0.2 ± 0.01 μm. Material properties are given in [15, 16]. For this material, only B3B tests were carried out since in-house derived ROR data for specimens with thicknesses of 2 mm are already available in the literature [17].

The thickness of all samples was measured using a micrometer IP65 (Mitutoyo) associated with a measurement uncertainty of ~ 2 μm, yielding thicknesses that deviated slightly from the nominal values given in Table 1. In the results and discussion section, the fracture stress values and their distributions are discussed with respect to the real sample thicknesses.

A B3B test set-up was designed with the objective to evaluate the strength of thin ceramic specimens in

Table 1 Different test series for ALUMINA1, ALUMINA2 and Spinel

Material	Test series	Number of specimens	Nominal sample thickness [μm]	Testing method
ALUMINA1	A1	40	120	B3B
	B1	40	250	B3B
	C1	45	800	ROR
ALUMINA2	A2	40	120	B3B
	B2	40	250	B3B
	C2	45	800	ROR
Spinel		35	200	B3B

a thickness range between 60 and 300 μm. Due to this anticipated specimen thickness range, ball radii of 1 mm were chosen, based on the three main criteria for the B3B test outlined in the work of Börger et al. [7]. The stated ball radii should, therefore, lead to a support radius of ∼ 1.155 mm following the equation given in [7]. Based on the boundary conditions and the estimated fracture loads in the mN to N range [18], the B3B set-up was designed for use in a micro-indentation system (CSM, Anton Paar), see also Fig. 1.

The loading ball was produced from a sapphire rod with one end being rounded resulting in a hemispherical probe of 1 mm radius. Potential frictional effects can be neglected since the support balls are able to roll freely. In addition, to further reduce the friction, the support balls rest on a glass plate. The movement of the support balls was aided by a stainless steel containment plate surrounding them, while unnecessary movement of the support balls in- and outward was also prevented, following suggestions given in [19].

The tests were carried out with a loading rate of 5 N/min. The specimens' central deflections, i.e., the displacement of the rod, and the loads were continuously recorded, as exemplified in Fig. 2. The rather nonlinear behavior at very low loads (< 1 N) can be attributed to initial settlement of the measurement system and is followed by a linear increase of the slope, indicating elastic deformation until fracture occurs. Note, some specimens still sustained load after initial crack growth, since the specimens were not fully fractured. However, the low compliance of the failed specimens led to large deflections with decreasing sustainable loads. The fracture initiations, visible in terms of load–displacement curves as deviations from linear elastic behavior, were used in the subsequent calculation of fracture stresses and Weibull analysis.

Based on the critical failure load F, the fracture stress σ_f for B3B tested specimens was calculated using the following relationship [19]:

$$\sigma_f = f\left(\frac{R_a}{R}, \frac{t}{R}, v\right) \cdot \frac{F}{t^2} \qquad (1)$$
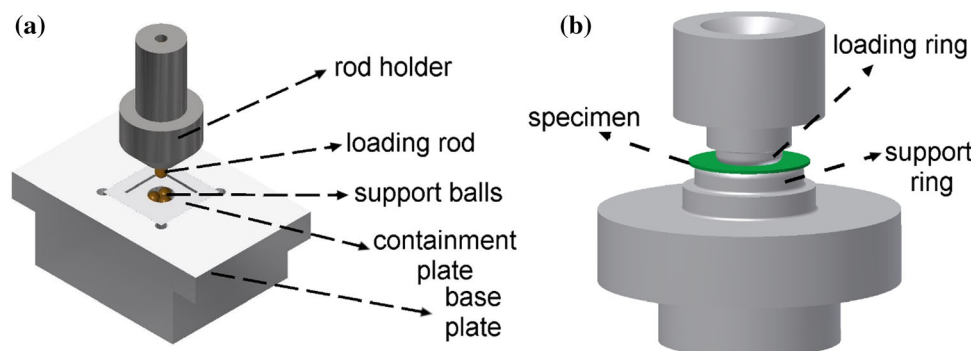

Figure 1 a Schematic representation of the B3B test set-up, adapted for usage in a micro-indenter system (CSM, Anton Paar). The support balls are enclosed by a containment plate in order to prevent outward movement and rest on a glass plate to minimize friction. **b** Schematic of the ROR test set-up, see also [14, 16].
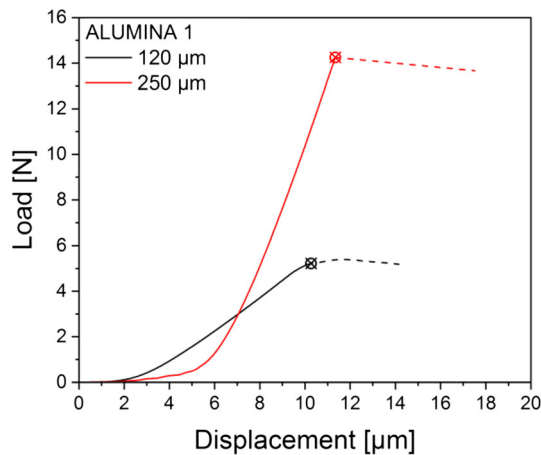
Figure 2 Typical load–displacement curves recorded during the B3B testing of Al$_2$O$_3$ specimens. The apparent fracture loads are indicated by the square symbols. Nonlinear behavior at the beginning of the measurement (< 1 N) can be attributed to the settlement of the test system.

where t is the thickness of the specimen, v the Poisson ratio, R_a the support radius, and R the sample radius. The expression $f\left(\frac{R_a}{R}, \frac{t}{R}, v\right)$ is a dimensionless function, which can be derived by an online tool based on finite element (FE) modeling made available by the University of Leoben [7, 20].

In contrast to the B3B tests, the ROR tests were performed using an electromechanical testing machine (INSTRON 1362), using similar procedures as outlined in [21–23]. The load was measured using a $\pm$ 1000 N load cell (Lebow Corporation) and the displacement by a linear variable differential transformer (Solartron Metrology) with the aid of a ceramic extension rod. In order to carry out the ROR tests, the samples were placed on a fixed Alumina support ring, and the load was applied with a loading rate of 1000 N per minute by an Alumina loading ring placed on the sample. The fracture stress σ_f was calculated using linear bending theory [24]:

$$\sigma_f = \frac{3(1+v)F}{2\pi t^2}\left[\ln\left(\frac{D_s}{D_l}\right) + \left(\frac{1-v}{1+v}\right)\left(\frac{D_s^2 - D_l^2}{2D^2}\right)\right] \quad (2)$$

where F is the fracture load, v the Poisson's ratio, t the thickness, D the diameter of the sample, D_l the diameter of the loading ring, and D_s the diameter of the support ring. The geometries were chosen based on the boundary conditions, as outlined in [25], which were satisfied by sample thicknesses of $\sim$ 800 μm and ring diameters of $D_l = 3.34$ and $D_s = 8.086$ mm, respectively.

Based on the determined fracture stress values, Weibull statistical analyses' were performed using [26]:

$$P_f = 1 - \exp\left[-\left(\frac{\sigma_f}{\sigma_0}\right)^m\right] \quad (3)$$

where P_f is the failure probability. The characteristic strength σ_0 is equivalent to the fracture stress for a failure probability of 63.2%, and m is the Weibull modulus, which describes the variability of the fracture stresses. A linear fitting procedure was implemented for the analysis. The obtained Weibull modulus as well as the 95% confidence interval were corrected to consider the number of tested specimens N following the relation:

$$m_{corr} = b \cdot m \quad (4)$$

where m_{corr} is then the corrected Weibull modulus, and b is a correction factor depending on N, which was derived from the corresponding standard [27]. In general, since the probability of a defect being present in a specimen depends on either the volume or surface area of the assessed materials (associated with the effect of either dominating volume defects or surface defects), the fracture strength of a material is affected by the size of the tested specimen as well as by potential stress gradients related to the testing method. Hence, the derived fracture strength has to be associated with an effective volume in the case of volume defects, V_{eff}, while in case of surface defects the effective area, S_{eff}, needs to be considered [10, 25]. The effective surface and effective volume are computed based on "principle of independent action" (PIA-criterion) [13, 28]. In case of the B3B test, the effective volume V_{B3B} as well as the effective area S_{B3B} can be calculated using a FE-model-based software tool that integrates the stresses over the finite elements [4, 20]. The value of V_{eff} and S_{eff} of the ROR test specimen can be calculated by expressions given in [29]. Using V_{eff} or S_{eff}, the material strength can be rescaled for different volumes or areas based on the Weibull theory [25]:

$$\sigma_{0,1} = \sigma_{0,2}\left(\frac{V_{eff,2}}{V_{eff,1}}\right)^{\frac{1}{m}} \quad (5)$$

$$\sigma_{0,1} = \sigma_{0,2}\left(\frac{S_{eff,2}}{S_{eff,1}}\right)^{\frac{1}{m}} \quad (6)$$

where $\sigma_{0,1}$ and $\sigma_{0,2}$ are the characteristic strength of the specimens for the considered testing geometry 1

and 2, corresponding in the current work to B3B and ROR, respectively. The associated effective volumes and effective areas are $V_{eff,1}$, $V_{eff,2}$ and $S_{eff,1}$, $S_{eff,2}$, respectively. In order to conclusively determine the dominant failure causing defect type, fractographic analysis are necessary. Therefore, SEM images of the fractured surfaces have been obtained using a Zeiss Merlin scanning electron microscopy instrument (Carl Zeiss Microscopy, Oberkochen, Germany). The critical flaw size α was estimated using the equation [30]:

$$\alpha = \frac{1}{\pi}\left(\frac{K_{IC}}{\sigma}\right)^2 \qquad (7)$$

where K_{IC} is the fracture toughness given in the corresponding product data sheet and literature [14, 16].

Results and discussion

The results of the individual ALUMINA test series are summarized in Table 2. For ALUMINA1, Weibull moduli of all three test series (for B3B and ROR) are in good agreement, indicating that the fracture stress distributions are comparable. The same holds true for the individual test series results for ALUMINA2.

The characteristic strengths should decrease with increasing effective volume or surface area. A graphical representation of a double logarithmic plot of the characteristic strengths as a function of the effective volume or the effective surface area should reveal a linear dependency. The slope of this linear regression is equivalent to the Weibull modulus. The respective plots for the two ALUMINA materials are presented in Fig. 3. All results are well described by a linear trend line (red line) reflecting the validity of the data of each individual test series (Table 2). However, the Weibull moduli derived from the linear regression over all test series are slightly lower, compared

to the values obtained for the individual test series. These lower values indicate that this might be a more conservative approach to predict the failure probability of larger components. Overall, the Weibull modulus of the individual test series is in good agreement with the one based on the effective volume approach (Fig. 3a, c). Therefore, volume defects appear to be the likely failure origin.

However, conclusions with respect to the dominant failure causing defect type should not be based only on statistical approaches. The failure origin was, therefore, further investigated by fractography. Representative SEM images of the fracture surface of the ALUMINA1 test series are show in Fig. 4, corresponding images of the ALUMINA2 samples are given in the supplementary material. In all alumina samples, the reason of failure seems to be pores near the sample surface. Based on Eq. (7), the critical flaw size α_c is calculated for each test series, values are summarized in Table 3. The calculated critical flaw sizes are in good agreement with the actual observed fracture origin sizes.

For both Alumina materials, the Weibull moduli are, within the limits of uncertainty, in reasonable agreement with the values given in the supplier's data sheet [14]. However, the fracture strengths given in the data sheet are slightly higher compared to the ROR derived values (Table 2). Hence, the effective volume in their work might be slightly lower compared to our ROR samples.

For the spinel specimens, Table 4 summarizes the Weibull analysis results of the B3B along with the ROR-based results from [16]. The Weibull moduli agree reasonably well within the limits of uncertainty, however, as expected, the characteristic strength is significantly lower when derived from ROR tests compared to the B3B data.

The characteristic strengths of $MgAl_2O_4$ are presented in Fig. 5a, b as a function of the effective volume and effective surface area, respectively. For

Table 2 ALUMINA1 and 2, average thickness t, characteristic strength σ_0 and Weibull moduli m_{corr} with the upper and lower limits of the confidence intervals, average effective volume V_{eff} and effective surface area S_{eff}

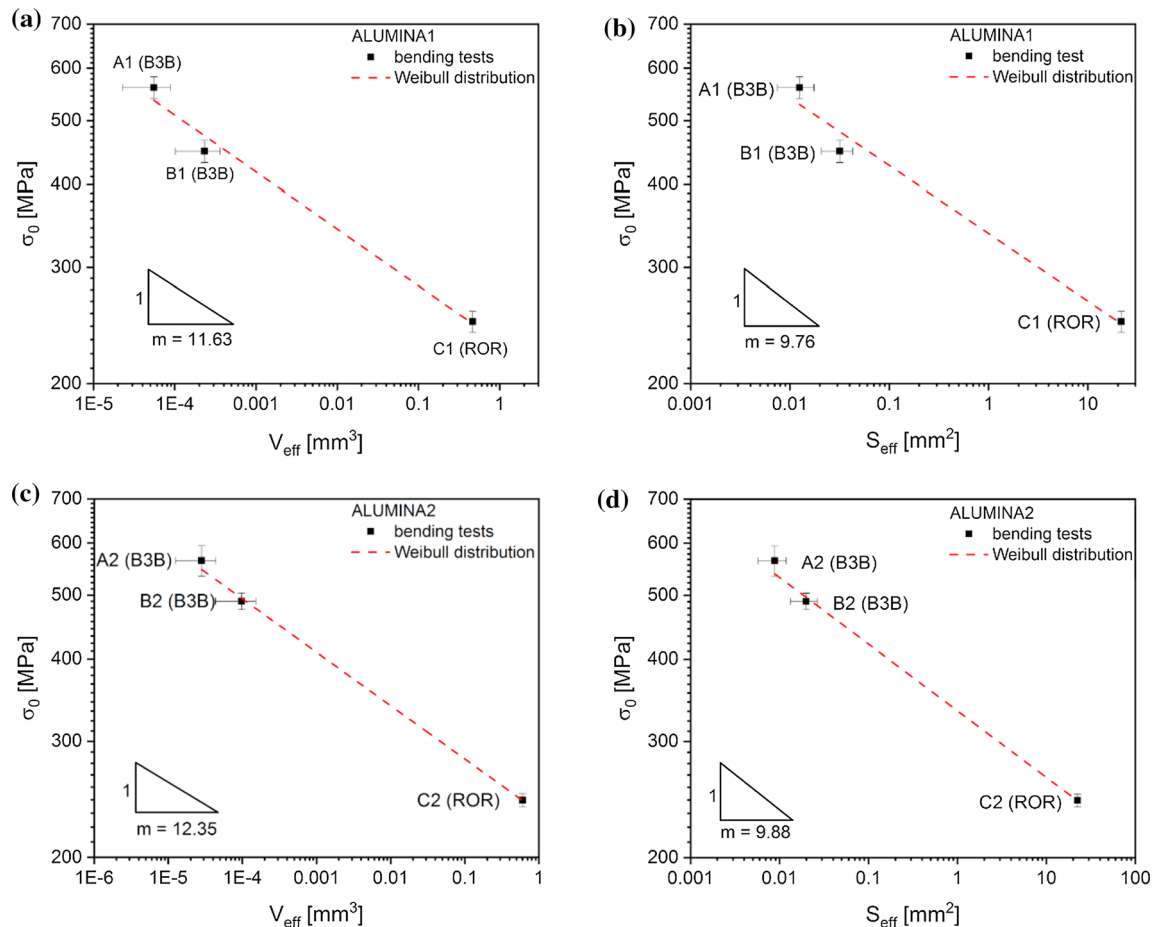| Test series	t [μm]	σ_0 [MPa]	m_{corr} [−]	V_{eff} [mm^3]	S_{eff} [mm^2]
A1 (B3B)	120 ± 10.0	561^{572}_{550}	$16.7^{20.4}_{12.5}$	$5.5 \times 10^{-5} \pm 3.3 \times 10^{-5}$	0.012 ± 0.005
B1 (B3B)	263 ± 6.2	449^{458}_{441}	$16.0^{19.4}_{12.1}$	$2.3 \times 10^{-4} \pm 1.3 \times 10^{-4}$	0.03 ± 0.01
C1 (ROR)	836 ± 7.4	248^{253}_{244}	$17.6^{21.4}_{13.2}$	0.465 ± 0.003	$21.6 \pm 4 \times 10^{-5}$
A2 (B3B)	151 ± 9.2	564^{579}_{549}	$12.0^{14.7}_{9.0}$	$2.8 \times 10^{-5} \pm 1.6 \times 10^{-5}$	0.009 ± 0.003
B2 (B3B)	246 ± 8.1	489^{496}_{483}	$19.0^{22.6}_{15.0}$	$9.7 \times 10^{-5} \pm 5.4 \times 10^{-5}$	0.02 ± 0.007
C2 (ROR)	843 ± 6.2	244^{250}_{238}	$14.0^{17.1}_{10.5}$	0.6 ± 0.003	$22.4 \pm 4.7 \times 10^{-5}$

Figure 3 Characteristic strengths of material ALUMINA1 as a function of the effective volume in (**a**) and effective surface areas in (**b**) Likewise for ALUMINA2, the characteristic strength as a function of the effective volume in (**c**) and the effective surface in (**d**). The used testing method B3B or ROR, respectively, is given in brackets. The red line represents a linear regression based on the respective 3 test series. The slope of this regression being equivalent to the Weibull modulus is presented at the bottom left corner.

the spinel, only two test series are available. A linear regression based on only two datasets will always result in a perfect fit. According to the Weibull theory, the slope of the linear regression should be equivalent to the Weibull modulus. Indeed the slope derived values presented in Fig. 5 based on the effective volume is 7.6, and the value based on the effective surface is 6.1. Both of these values agree well within the limits of uncertainty with the individual test series results. Therefore, a linear dependency between the ROR and B3B results is confirmed. Overall, again the agreement of the effective volume approach with the Weibull moduli of the individual test series is better, indicating volume defects are more likely.

The statistical analysis based on different effective volumes, as presented here for volumes covering more than three orders of magnitude, can be used to give an accurate extrapolation of fracture stresses for particular failure probabilities of components with application relevant dimensions. Small scale pores within the $MgAl_2O_4$ have been reported as the reason of failure in the ROR tests [15]. SEM images of the $MgAl_2O_4$ specimens' fractured surfaces after B3B testing have been made (Fig. 6). The main failure causing defect seems to be coarse-grained agglomerates and associated microcracks. Therefore, volume defects seem to be the main failure causing defect type for the $MgAl_2O_4$ specimens in the ROR as well as the B3B test.
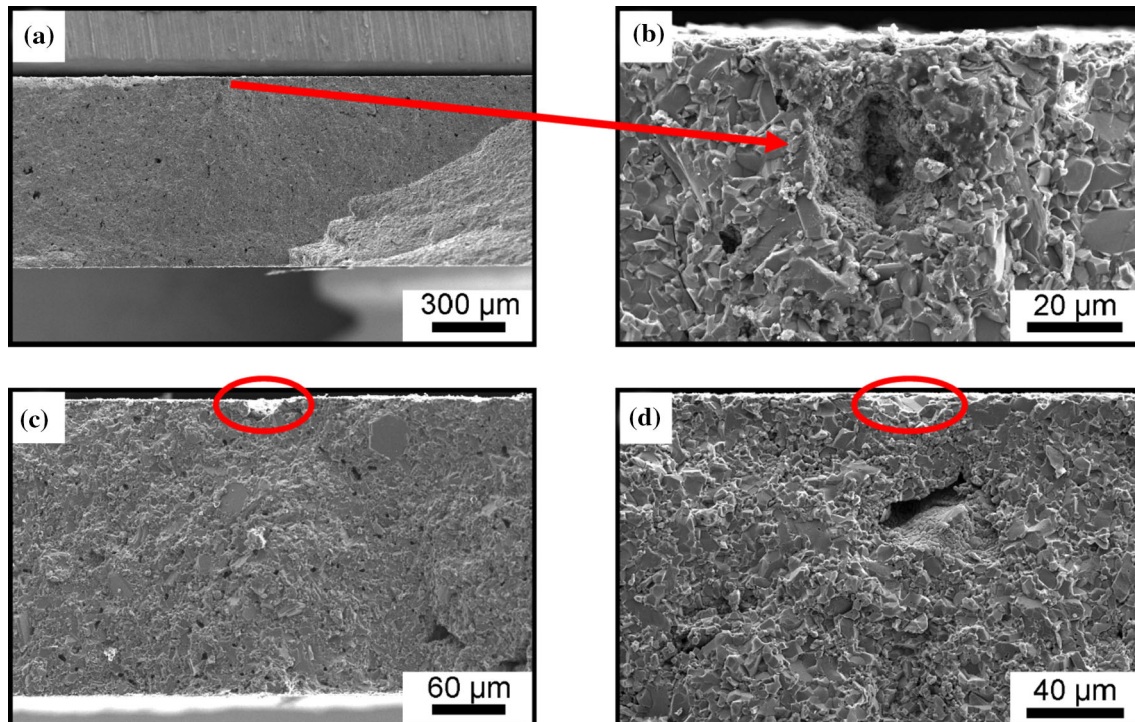
Figure 4 Representative SEM images of the fracture surfaces of ALUMINA1 specimens (tension side at the top). **a** Fracture surfaces after ROR testing (C1 test series), **b** at higher magnification, **c** B1 test series (after B3B test), **d** A1 test series (after B3B test). In all fracture surfaces, pores are the most likely failure origins.

Table 3 Summary of the calculated critical flaw sizes and observed fracture origin sizes of the selected ALUMINA test series specimens

Material	Test series	α_c [μm]	Fracture origin size [μm]
ALUMINA1	A1 (B3B)	8	8
	B1 (B3B)	12	12
	C1 (ROR)	40	38
ALUMINA2	A2 (B3B)	8	9
	B2 (B3B)	10	12
	C2 (ROR)	42	40

Conclusion

The fracture test methodology based on a combination of ball-on-3-ball and ring-on-ring tests using a custom-designed miniaturized ball-on-3-ball test setup was evaluated. The evaluation was based on the analysis of experimentally derived fracture stress data for different ceramic materials and an associated Weibull statistics. The analyses of the characteristic strengths as a function of the effective volume and effective area were in good agreement with the values derived from the analysis of the individual data sets for all materials. The agreement of the effective volume approach with the Weibull moduli of the individual test series was better, indicating volume defects are more likely, confirmed by the fractographic analysis. The illustrated considerations highlight the possibility to derive fracture stresses for application relevant ceramic components, from smaller or larger test bodies, even if different fracture test methods are used, as long as associated statistical analysis' on basis of the effective volume or effective

Table 4 $MgAl_2O_4$, average thickness t, characteristic strength σ_0 and Weibull moduli m_{corr} with the upper and lower limits of the confidence intervals, average effective volume V_{eff} and effective surface area S_{eff}. ROR from [16]

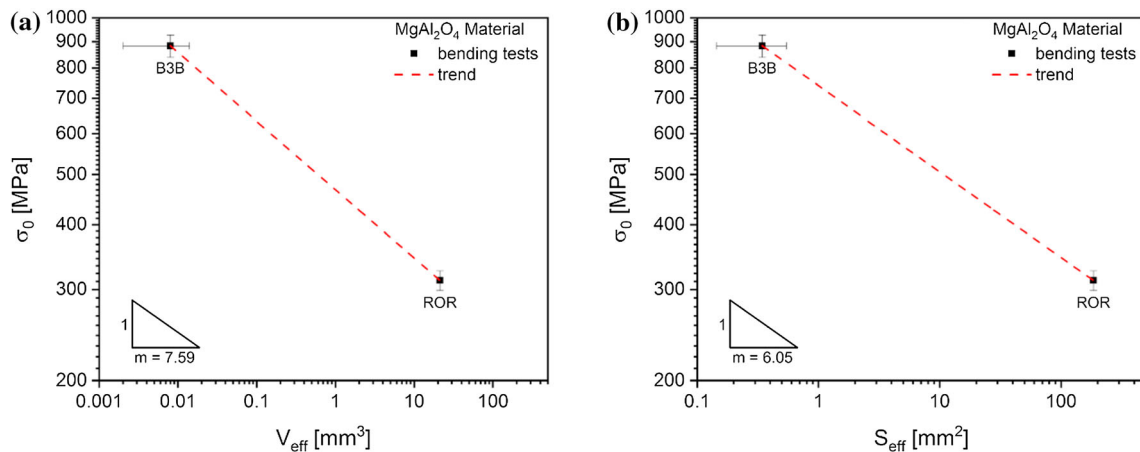| Specimen	t [μm]	σ_0 [MPa]	m_{corr} [−]	V_{eff} [mm^3]	S_{eff} [mm^2]
B3B	193 ± 3	883^{926}_{841}	$6.4^{8.0}_{4.9}$	0.008 ± 0.006	0.3 ± 0.2
ROR	2000 ± 200	312^{326}_{299}	$7.7^{9.5}_{5.8}$	21.1 ± 1.7	185 ± 0.2

Figure 5 Comparison of the ROR and B3B derived characteristic strength results as a function of the effective volume in (**a**) and effective area in (**b**). The red line represents the linear regression. Generally, a regression between only 2 data has limited meaning, but following the Weibull theory the slope of this regression is equivalent to the Weibull modulus. Hereby slope values agreeing well with the Weibull moduli of the individual test series confirm the linear dependency.
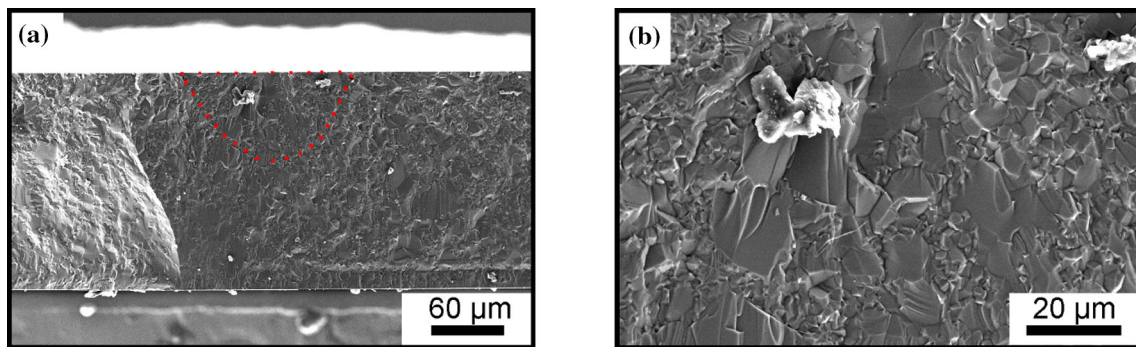

Figure 6 SEM images of the fractured $MgAl_2O_4$ surface after B3B testing. In (**a**), the red circle highlights an area with radial orientated microcracks, originating from coarse-grained agglomerates shown in (**b**).

surface are applied. These findings are, therefore, a solid foundation for the prediction of failure probabilities of application relevant ceramic components. The combination of a micro-indentation system and the ball-on-3-ball test represents an easy, fast and reliable method to investigate the fracture behavior of small scale ceramic materials.

Supplementary Information: The online version contains supplementary material available at http s://doi.org/10.1007/s10853-022-07143-6.

Acknowledgements

Funding

References

[1] Zhao Y-Y, Ma E, Xu J (2008) Reliability of compressive fracture strength of Mg–Zn–Ca bulk metallic glasses: flaw sensitivity and Weibull statistics. Scr Mater 58(6):496–499

[2] Lu C, Danzer R, Fischer FD (2002) Fracture statistics of brittle materials: weibull or normal distribution. Phys Rev E 65(6):067102

[3] Harrer W, Danzer R, Supancic P, Lube T (2009) Influence of the sample size on the results of B3B-tests. Key Eng Mater 409:176–184

[4] Nohut S (2012) A general formulation for strength prediction of advanced ceramics by ball-on-three-balls (B3B)-test with different multiaxial failure criteria. Ceram Int 38(3):2411–2420

[5] de With G, Wagemans HH (1989) Ball-on-ring test revisited. J Am Ceram Soc 72(8):1538–1541

[6] Morrell R, McCormick N, Bevan J, Lodeiro M, Margetson J (1999) Biaxial disc flexure–modulus and strength testing. Br Ceram Trans 98(5):234–240

[7] Börger A, Supancic P, Danzer R (2002) The ball on three balls test for strength testing of brittle discs: stress distribution in the disc. J Eur Ceram Soc 22(9–10):1425–1436

[8] Gruber M, Kraleva I, Supancic P, Danzer R, Bermejo R (2020) A novel approach to assess the mechanical reliability of thin, ceramic-based multilayer architectures. J Eur Ceram Soc 40:4727–4736

[9] Danzer R, Supancic P, Pascual J, Lube T (2007) Fracture statistics of ceramics–Weibull statistics and deviations from Weibull statistics. Eng Fract Mech 74(18):2919–2932

[10] Gross D, Seelig T (2017) Fracture mechanics: with an introduction to micromechanics. Springer

[11] Wang CH (1996) Introduction to fracture mechanics. DSTO Aeronautical and Maritime Research Laboratory Melbourne, Australia

[12] Bazant ZP, Planas J (1997) Fracture and size effect in concrete and other quasibrittle materials. CRC Press

[13] Staudacher M, Lube T, Schlacher J, Supancic P (2021) Comparison of biaxial strength measured with the ball-on-three-balls-and the ring-on-ring-test. Open Ceram 6:100101

[14] CeramTec (2019) Kenndatenblatt ALOTEC®

[15] Von Helden S (2020) Mechanische Eigenschaften transparenter Keramik im Vergleich mit gehärteten und ungehärteten Gläsern. Dissertation/PhD Thesis, Rheinisch-Westfälische Technische Hochschule Aachen, Aachen

[16] Von Helden S, Malzbender J, Krüger M (2019) Mechanical properties, wear resistance and surface damage of glasses and $MgAl_2O_4$ spinel ceramic after abrasion and scratch exposure. Ceram Int 45(8):10765–10775

[17] Von Helden S, Krüger M, Malzbender J (2019) Strength of transparent ceramic composites with spinel. J Mater Sci 54(24):14666–14676

[18] Hemker KJ, Sharpe WN Jr (2007) Microscale characterization of mechanical properties. Annu Rev Mater Res 37:93–126

[19] Börger A, Supancic P, Danzer R (2004) The ball on three balls test for strength testing of brittle discs: part II: analysis of possible errors in the strength determination. J Eur Ceram Soc 24(10–11):2917–2928

[20] Börger A, Supancic P, Danzer R (2011) Ball on 3 balls- test (web-app). Available: http://www.isfk.at/de/960

[21] Yan G, Nonemacher JF, Zheng H, Finsterbusch M, Malzbender J, Krüger M (2019) An investigation on strength distribution, subcritical crack growth and lifetime of the lithium-ion conductor $Li_7La_3Zr_2O_{12}$. J Mater Sci 54(7):5671–5681

[22] Huang B, Malzbender J, Steinbrech R, Singheiser L (2009) Mechanical properties of $La_{0.58}Sr_{0.4}Co_{0.2}Fe_{0.8}O_{3-\delta}$ membranes. Solid State Ion 180(2–3):241–245

[23] Pećanac G, Foghmoes S, Lipińska-Chwałek M, Baumann S, Beck T, Malzbender J (2013) Strength degradation and failure limits of dense and porous ceramic membrane materials. J Eur Ceram Soc 33(13–14):2689–2698

[24] ASTM (2003) C1499 standard test method for monotonic equibiaxial flexural strength of advanced ceramics at ambient temperature. In: annual book of ASTM standards, ASTM international, West Conshohocken

[25] ASTM (2007) C1239 standard practice for reporting uniaxial strength data and estimating Weibull distribution parameters

for advanced ceramics, In: annual book of ASTM standards, ASTM international, West Conshohocken

[26] Malzbender J, Steinbrech R, Singheiser L (2009) Failure probability of solid oxide fuel cells. Ceram Eng Sci Proc 26:293–298

[27] Din E (2007) 843-5. Hochleistungskeramik—Mechanische Eigenschaften Monolithischer Keramik bei Raumtemperatur—Teil 5: Statistische Auswertung. DIN Deutsches Institut für Normung ev, Berlin

[28] Barnett RL, Hermann PC, Wingfield JR, Connors CL (1967) Fracture of brittle materials under transient mechanical and thermal loading. IIT Research Institute, Chicago

[29] ASTM (2010) C1683 standard practice for size scaling of tensile strengths using weibull statistics for advanced ceramics, In: annual book of ASTM standards, ASTM international, West Conshohocken

[30] Kingery WD, Bowen HK, Uhlmann DR (1976) Introduction to ceramics. Wiley